AJ, in press
Preprint typeset using LaTeX style emulateapj v. 5/2/11

arXiv:1203.5588v1 [astro-ph.CO] 26 Mar 2012

STRUCTURAL PARAMETERS FOR GLOBULAR CLUSTERS IN THE OUTER HALO OF M31

Song Wang,[1,2,3] Jun Ma[1,3]

AJ, in press

ABSTRACT

In this paper, we present internal surface brightness profiles, using images in the F606W and F814W filter bands observed with the Advanced Camera for Surveys on the *Hubble Space Telescope*, for ten globular clusters (GCs) in the outer halo of M31. Standard King models are fitted to the profiles to derive their structural and dynamical parameters. The results show that, in general, the properties of clusters in M31 and the Milky Way fall in the same regions of parameter spaces. The outer halo GCs of M31 have larger ellipticities than most of GCs in M31 and the Milky Way. Their large ellipticities may be due to galaxy tides coming from satellite dwarf galaxies of M31 or may be related to the apparently more vigorous accretion or merger history that M31 has experienced. The tight correlation of cluster binding energy E_b with mass $M_{\rm mod}$ indicates that, the "fundamental plane" does exist for clusters, regardless of their host environments, which is consistent with previous studies.

Subject headings: galaxies: individual (M31) – galaxies: halos – globular clusters: general

1. INTRODUCTION

The mechanisms involved in galaxy formation is still one of the major unsolved problems in astrophysics (e.g., Perrett et al. 2002). Globular clusters (GCs), which are considered to be debris of the galaxy formation, have a record about the information on both their formation condition and dynamical evolution within the environment of their host galaxies, which are reflected by their spatial structures and kinematics (Barmby et al. 2007; Mclaughlin et al. 2008). So, GCs are regarded as a laboratory of galaxy history (Brodie & Strader 2006). In addition, GCs can be used as one of excellent tracers of substructures in the outer regions of their parent galaxies. For example, Bellazzini et al. (2003) identified the accretion signature of the Sagittarius dwarf galaxy among the GCs in the outer halo of the Milky Way (MW); Mackey et al. (2007) found some of the GCs in the outer halo of M31 are rather unlike their MW counterparts as they are metal-poor, compact, and very luminous, which may well offer important clues to differences in the early formation and evolution of the two galaxies or in their subsequent accretion histories (see Mackey et al. 2007, for details). Thus, a detailed study of GCs in the outer halo of a galaxy is important.

M31, with a distance of ∼ 780 kpc from us (Stanek & Garnavich 1998; Macri 2001), is the largest galaxy in the Local Group, and it is so close to us that the GCs in it can be well resolved with the cameras on the *Hubble Space Telescope* (*HST*). M31 contains more GCs than all other Local Group galaxies combined with 654 confirmed GCs and 606 GC candidates in the version V4.0 of the Revised Bologna Catalogue (RBC) of M31 GCs (Galleti et al. 2004, 2006, 2007, 2009). M31 contains so many GCs that a variety of clusters may be included such as classic globulars, extended and diffuse globulars (Huxor et al. 2008), intermediate-age globulars (Puzia et al. 2005; Fan et al. 2006; Ma et al. 2009; Wang et al. 2010) and young massive clusters (Perina et al. 2009, 2010; Ma et al. 2011). GCs in the outer halo of M31 have been discussed by many authors (Martin et al. 2006; Mackey et al. 2006, 2007, 2010; Huxor et al. 2008), which may provide important clues for the accretion and interaction events between M31 and surrounding galaxies. Recently, Mackey et al. (2010) found a genuine physical association between GCs and multiple tidal debris streams in the outer regions of M31, implying that the remote GC system of M31 was largely accreted from the satellite galaxies (also reported in Huxor et al. 2011).

Structures and kinematics of GCs can be determined by fitting different models to the surface brightness profiles, combined with mass-to-light ratios (M/L values) estimated from velocity dispersions or population-synthesis models. In general, three models are used in the fits: the simple model of single-mass, isotropic, modified isothermal sphere developed by King (1966), an alternate modified isothermal sphere based on the ad hoc stellar distribution function of Wilson (1975), and the $R^{1/n}$ surface-density profile of Sérsic (1968). With these models, many authors have achieved some success in determining structures and kinematics of clusters from different galaxies, using images from ground-based telescopes or *HST*: the MW (Trager et al. 1993, 1995; Mclaughlin & van der Marel 2005); the Large and Small Magellanic Clouds, Fornax and Sagittarius dwarf spheroidal galaxies (Mackey & Gilmore 2003a,b,c; Mclaughlin & van der Marel 2005); M31 (Grillmair et al. 1996; Barmby et al. 2002, 2007, 2009; Ma 2011; Ma et al. 2006, 2007, 2012; Federici et al. 2007; Strader et al. 2009; Huxor et al. 2011); M33 (Larsen et al. 2002); NGC 5128 (Holland et al. 1999; Harris et al. 2002; Martini & Ho 2004; Mclaughlin et al. 2008). A number of studies focusing on the correlations between cluster parameters have been performed, which showed that there exists a fundamental plane among

---

[1] National Astronomical Observatories, Chinese Academy of Sciences, Beijing, 100012, China;
majun@nao.cas.cn
[2] Graduate University, Chinese Academy of Sciences, Beijing, 100039, China
[3] Key Laboratory of Optical Astronomy, National Astronomical Observatories, Chinese Academy of Sciences, Beijing, 100012, China

most clusters, regardless of their different "growing environment" in different host galaxies.

Barmby et al. (2007) derived structural parameters for 34 GCs in M31 based on *HST* Advanced Camera for Surveys (ACS) observations, and the derived structural parameters were combined with corrected versions of those measured in an earlier survey in order to construct a comprehensive catalog of structural and dynamical parameters for 93 M31 GCs. Barmby et al. (2009) measured structural parameters for 23 bright young clusters in M31 based on the *HST* Wide Field Planetary Camera 2 (WFPC2) observations, and suggested that on average they are larger and more concentrated than typical old clusters. However, the sample clusters from Barmby et al. (2007) and Barmby et al. (2009) lie at projected radii $R_p < 20$ kpc except for five clusters G001, G002, G339, G353 and B468, the projected radii of which are 34.55, 33.62, 28.68, 26.32 and 20.05 kpc, respectively; and most of the sample clusters lie at projected radii $R_p < 10$ kpc. So, structural parameters for GCs in the outer halo of M31 are worthwhile to be determined. In addition, Huxor et al. (2011) derived structural parameters for 13 extended clusters (ECs) in the halo regions of M31 by fitting the King (1962) profiles to the photometry data taken with the Wide Field Camera on the Isaac Newton Telescope (INT) and MegaCam on the Canada-France-Hawaii Telescope, which may provide an interesting comparison with the structural parameters for GCs in the outer halo of M31.

In this paper, we determined spatial structures and kinematics for ten GCs in the outskirts of M31. In Section 2, we give observations of the sample GCs and the data-processing steps to derive their surface brightness profiles. In Section 3, we determine structures and kinematics of the sample clusters with the model fitting. In Section 4, we discuss correlations of the structural and kinematic parameters of the sample clusters here combining with those of the Galactic and M31 clusters studied by other authors. Finally, we give our summaries in Section 5.

2. DATA AND ANALYSIS METHOD

2.1. *Globular Cluster Sample*

As mentioned in the introduction, a detailed study of GCs in the outer halo of a galaxy is important, since they can serve as one of excellent tracers of substructures in the outer regions of their parent galaxy. Till now, for M31, most of the clusters whose structural parameters have been determined, lie at projected radii $R_p < 10$ kpc. So, structural parameters for GCs in the outer halo of M31 are worthwhile to be measured. In this paper, detailed studies of the structures of a sample of ten GCs in the outer halo of M31 from Mackey et al. (2007) will be presented. These sample halo GCs are interesting. For example, Mackey et al. (2007) found some of them are rather unlike their MW counterparts as they are metal-poor, compact, and very luminous (see Mackey et al. 2007, for details). Eight of the ten halo GCs lie at projected radii $R_p > 30$ kpc, of which two lie at very large distances from M31: $R_p \sim 78$ and 100 kpc, respectively. In addition, Mackey et al. (2007) estimated their metallicities, distance moduli and reddening values by fitting the Galactic GC fiducials from Brown et al. (2005) to their observed color-magnitude diagrams in the F606W and F814W filters of deep images observed with the the ACS Wide Field Camera (WFC) under the *HST* program GO-10394 (PI: Tanvir). This program was aimed to obtain deep high resolution photometry of outer halo GCs in M31 to study their stellar populations, line-of-sight distances and structural parameters. Targets were imaged in the F606W and F814W filters for ~ 1800s and ~ 3000s, respectively, with small dithers between various sub-exposures (Richardson et al. 2009).

2.2. *Surface Brightness Profiles*

We used the analogous procedure adopted by Barmby et al. (2007) to produce surface brightness profiles with ELLIPSE in IRAF. The center positions of these clusters were determined by centroiding. Elliptical isophotes were fitted to the observed data, with no sigma clipping. Two passes of ELLIPSE task were run in the procedure. In the first pass, ellipticity and position angle (P.A.) were allowed to vary with the isophote semimajor axes; in the second pass, surface brightness profiles were derived on fixed, zero-ellipticity isophotes, meaning that we always had circularly symmetric intensity profiles, which would be fitted with circular structure models. The overall ellipticity and position angle were determined by averaging the ELLIPSE output over the isophotal semimajor axes, and the uncertainty is σ . Table 1 lists the average ellipticity, P.A. and some additional integrated data for the sample GCs. VI magnitudes of 9 GCs and I magnitude of GC6 are from Huxor et al. (2008), while V magnitude of GC6 is from Reed et al. (1992). The galactocentric distances, distance moduli, reddening values and metallicities are from Mackey et al. (2007), while the uncertainties of [Fe/H] are assumed to be 0.6 as Barmby et al. (2000) suggested for the standard deviation of the metallicity distribution of M31 GC system.

Raw output from package ELLIPSE is in terms of counts s^{-1} pixel^{-1}, which needs to multiply by 400 to convert to counts s^{-1} arcsec^{-1}, since the ACS/WFC spatial resolution is 0.05 arcsec pixel^{-1}. For drizzled ACS data, the units of counts are ELECTRONS (ACS Handbook). Two formulas were used to transform the ACS counts to surface brightness calibrated on the VEGAMAG system (ACS Handbook),

$$\mu_{\rm F606W}/{\rm mag\ arcsec^{-2}} = 26.398 - 2.5\log({\rm counts\ s^{-1}\ arcsec^{-1}}), \quad (1)$$

$$\mu_{\rm F814W}/{\rm mag\ arcsec^{-2}} = 25.501 - 2.5\log({\rm counts\ s^{-1}\ arcsec^{-1}}). \quad (2)$$

However, occasional oversubtraction of background during the multidrizzling in the automatic reduction pipeline leads to "negative" counts in some pixels, so we worked in terms of linear intensity instead of surface brightness in magnitudes. Given $M_{\odot,\rm F606W} = +4.64$, $M_{\odot,\rm F814W} = +4.14$[4], equations for transforming counts to surface brightness in intensity were derived (also see

---

[4] See http://www.ucolick.org/~cnaw/sun.html.

Barmby et al. 2007, for details),

$$I_{\rm F606W}/L_\odot \ {\rm pc}^{-2} \simeq 0.8427 \times ({\rm counts\ s^{-1}\ arcsec^{-1}}), \quad (3)$$

$$I_{\rm F814W}/L_\odot \ {\rm pc}^{-2} \simeq 1.2147 \times ({\rm counts\ s^{-1}\ arcsec^{-1}}). \quad (4)$$

Table 2 gives the final, calibrated intensity profiles for the ten clusters but with no extinction corrected. The reported F606W- and F814W-band intensities are calibrated on the VEGAMAG scale. Column (7) gives a flag for each point, which has the same meaning as Barmby et al. (2007) and Mclaughlin et al. (2008) defined.

2.3. *Point-spread Function*

As noted by Barmby et al. (2007) and Mclaughlin et al. (2008) that, though the sample GCs here are well resolved with ACS/WFC, the core structures are still influenced by the point-spread function (PSF). We convolved the structural models developed by King (1966) (hereafter 'King model') with a simple analytic description of the PSF before doing the model fitting, as given in Barmby et al. (2007),

$$I_{\rm PSF,F606W}/I_0 = [1 + (R/0.0686\ {\rm arcsec})^3]^{-3.69/3.0}, \quad (5)$$

and

$$I_{\rm PSF,F814W}/I_0 = [1 + (R/0.0783\ {\rm arcsec})^3]^{-3.56/3.0}, \quad (6)$$

with FWHMs of 0.125 arcsec and 0.145 arcsec in the F606W and F814W filters, respectively.

2.4. *Extinction and Magnitude Transformation*

When we fit models to the brightness profiles of the sample clusters, we will correct the inferred intensity profiles for extinction. The effective wavelengths of the ACS F606W and F814W filters are $\lambda_{\rm eff} \simeq 5918$ and 8060 Å (Sirianni et al. 2005). With the extinction curve A_λ taken from Cardelli et al. (1989) with $R_V = 3.1$, two formulas for computing $A_{\rm F606W}$ and $A_{\rm F814W}$ are derived: $A_{\rm F606W} \simeq 2.8\ E_{B-V}$; $A_{\rm F814W} \simeq 1.8\ E_{B-V}$. In addition, for easy comparison with catalogs of the GCs in the MW (see Section 4 for details), we transform the ACS/WFC magnitudes in the F606W filter to the standard V. Sirianni et al. (2005) has given transformations from WFC to standard $BVRI$ magnitudes both on observed and synthetic methods (see their Table 22). As synthetic transformations are based on larger color range and more safely employed, they should be considered the norm, unless some indicated cases (Sirianni et al. 2005). We used the synthetic transformation from F606W to V magnitude both on the VEGAMAG scale with a quadratic dependence on dereddened $(V-I)_0$. With the magnitudes in V and I bands and reddening values listed in Table 1, we found the $(V-I)_0$ values of all the sample clusters are larger than 0.4. So, the following transformation formula was applied here,

$$(V - {\rm F606W})_0 = -0.067 + 0.340(V-I)_0 - 0.038\ (V-I)_0^2, \quad (7)$$

for which we estimated a precision of about ±0.05 mag.

3. MODEL FITTING

There are a number of possible choices of structural models for fitting star cluster surface profiles, including King model, Wilson (1975), and Sérsic (1968), as mentioned in the introduction. King model is the most commonly used model in studies of star clusters. In addition, Barmby et al. (2007, 2009) found that M31 clusters are better fitted by King models. So, in this paper, the intensity profiles of the ten GCs in M31 will be fitted by King models defined by the phase-space distribution function,

$$f(E) \propto \begin{cases} \exp[-E/\sigma_0^2] - 1, & E < 0, \\ 0, & E \geq 0, \end{cases} \quad (8)$$

where E is the stellar energy, σ_0 is a velocity scale.

We first convolved King model with the ACS/WFC PSF for the F606W and F814W filters. Given a value for the scale radius r_0, we computed a dimensionless model profile $\widetilde{I}_{\rm mod} \equiv I_{\rm mod}/I_0$, and then carried out the convolution,

$$\widetilde{I}^*_{\rm mod}(R|r_0) = \iint_{-\infty}^{\infty} \widetilde{I}_{\rm mod}(R'/r_0)\widetilde{I}_{\rm PSF}\left[(x-x'),(y-y')\right]\ dx'\,dy'\ , \quad (9)$$

where $R^2 = x^2 + y^2$, and $R'^2 = x'^2 + y'^2$; and $\widetilde{I}_{\rm PSF}$ was approximated using the equations (5) and (6) (see Mclaughlin et al. 2008, for details). The observed surface brightness profiles were fitted by calculating and minimizing χ^2 as the sum of squared differences between model and observed intensities, with uncertainties listed in Table 2 being weights,

$$\chi^2 = \sum_i \frac{[I_{\rm obs}(R_i) - I_0\widetilde{I}^*_{\rm mod}(R_i|r_0) - I_{\rm bkg}]^2}{\sigma_i^2}, \quad (10)$$

in which a background $I_{\rm bkg}$ was also fitted.

Figure 1 displays the observed intensity profiles as a function of logarithmic projected radius and the best-fitting King model (solid red line) for each cluster. The observed data have been extinction corrected, following by a fitted $I_{\rm bkg}$ subtracted. The dashed blue lines represent the shape of the PSF for the WFC F606W or F814W filters. Most profiles of the sample clusters were well fitted by King model, except for those at the intermediate radii of GC3, GC7 and GC9. We checked the images, and found that the three clusters are very loose and there are several bright stars at the intermediate radii.

In Figure 1, open squares are ELLIPSE data points included in the least-squares model fitting, and the crosses are points flagged as 'DEP' or 'BAD', which are not used to constrain the fit. In this paper, the ELLIPSE gives isophotal intensities for 15 radii inside $R < 2$ pixels, however, all of them are derived from the same innermost 13 pixels, meaning that the isophotal intensities are not statistically independent. So, to avoid excessive weighting of the central regions of clusters in the fits, we only used intensities at radii $R_{\rm min}$, $R_{\rm min} + (0.5, 1.0, 2.0)$ pixels, or $R > 2.5$ pixels as Barmby et al. (2007) used. In addition, we deleted some individual isophotes which deviated strongly from their neighbours or showed irregular features by hand.

3.1. *Basic Model Parameters*

Table 3 lists the basic parameters of 20 model fits to the sample clusters here. Column (1) gives the cluster name, column (2) the detector/filter from which the observed data were derived. Column (3) gives the color

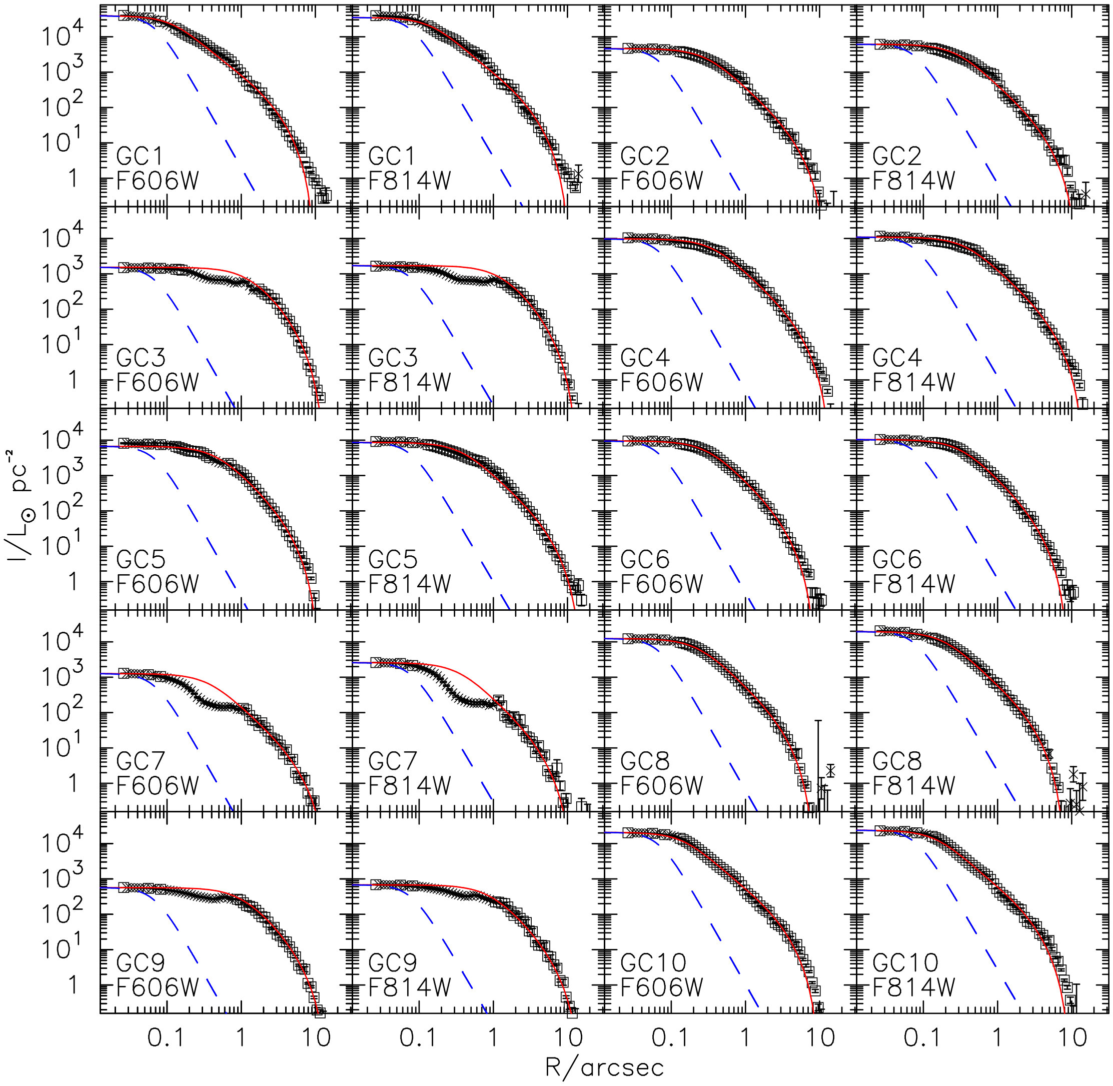

FIG. 1.— Surface brightness profiles and model fits for the sample GCs here.

correction $(V-\mathrm{F606W})_0$ to transform native instrumental magnitudes to the standard V scale. The fourth column shows the number of points in the intensity profile that are flagged as 'OK' in Table 2, which were used for constraining the model fits. Column (5) is the fitting model which is always King model here. Column (6) gives the minimum χ^2 obtained in the fits. Column (7) gives the best fitted background intensity. Column (8) gives the dimensionless central potential W_0 of the best-fitting model, defined as $W_0 \equiv -\phi(0)/\sigma_0^2$. Column (9) gives the concentration $c \equiv \log(r_t/r_0)$. Column (10) gives the best-fit central surface brightness in the native bandpass of the data. Column (11) and column (12) show the best model-fit scale radius r_0 in arcseconds and parsecs, respectively, while the latter was obtained from the angular scale with the distance moduli given in Table 1.

Uncertainties for the fitted model parameters were estimated following $\triangle\chi^2 \leq 1$ for 68% confidence intervals. However, as Barmby et al. (2007) pointed out, because the formal error bars estimated by ELLIPSE for the isophotal intensities are artificially small, the best-fit $\chi^2_{\rm min}$ can be exceedingly high ($\gg N_{\rm pts}$; the number of points used in the model fitting) even when a model fit is actually very good (see the values of $\chi^2_{\rm min}$ in Table 3), and this would result in unrealistically small estimates of parameter uncertainties. So, we also re-scale the χ^2 for all fitted models by a common factor chosen to make the global minimum $\chi^2_{\rm min} = (N_{\rm pts}-4)$ as Barmby et al. (2007) did. Under this re-scaling, the global minimum reduced χ^2 per degree of freedom is exactly one (see Barmby et al. 2007, for details).

3.2. *Derived Quantities*

Tables 4 and 5 give various derived parameters for the best-fitting models for each cluster (the details of their calculation are given by Mclaughlin et al. 2008).

The contents of Table 4 are:
Column (4): $\log r_t$, the model tidal radius in parsecs.
Column (5): $\log R_c$, the projected core radius of the model fitting a cluster, which is defined as $I(R_c) = I_0/2$.
Column (6): $\log R_h$, the projected half-light, or effective, radius of a model, containing half the total luminosity in projection.
Column (7): $\log(R_h/R_c)$, a measure of cluster concentration and relatively more model-independent than W_0

or c.
Column (8): $\log I_0 = 0.4(26.402 - \mu_{V,0})$, the best-fit central ($R = 0$) luminosity surface density in the V band, in units of $L_\odot$ pc^{-2}. The surface-brightness zero point of 26.402 corresponds to a solar absolute magnitude $M_{V,\odot} = +4.83$[5]. $\mu_{V,0}$ is derived from applying the term $(V - \mathrm{F606W})_0$ to the fitted central surface brightness in column (10) of Table 3.
Column (9): $\log j_0$, the central ($r = 0$) luminosity volume density in the V band in units of $L_\odot$ pc^{-3}.
Column (10): $\log L_V$, the V-band total integrated model luminosity, in units of $L_\odot$.
Column (11): $V_{\rm tot} = 4.83 - 2.5\log(L_V/L_\odot) + 5\log(D/10$ pc) is the total V-band magnitude of a model cluster.
Column (12): $\log I_h \equiv \log(L_V/2\pi R_h^2)$, the luminosity surface density averaged over the half-light/effective radius in the V band, in units of $L_{\odot,V}$ pc^{-2}.

The uncertainties of these derived parameters were estimated (separately for each given model family) by calculating them in each model that yields χ^2 within 1 of the global minimum for a cluster, and then taking the differences between the extreme and best-fit values of the parameters (see Mclaughlin & van der Marel 2005, for details).

The contents of Table 5 are:
Column (3): $\Upsilon_V^{\rm pop}$, the V-band mass-to-light ratio. The values of $\Upsilon_V^{\rm pop}$ were derived by applying the population synthesis models of Bruzual & Charlot (2003), assuming a Chabrier (2003) initial mass function (IMF) and age of 13 Gyr for all these clusters, with metallicities given in Table 1. Uncertainties of $\Upsilon_V^{\rm pop}$ include a ±2 Gyr uncertainty in age, as well as a ±0.6 uncertainty in [Fe/H].
Column (5): $\log M_{\rm tot} = \log\Upsilon_V^{\rm pop} + \log L_V$, the integrated cluster mass in solar units, estimated from the total model luminosity L_V.
Column (6): $\log E_b$, the integrated binding energy in ergs, which is defined as $E_b \equiv -(1/2)\int_0^{r_t} 4\pi r^2 \rho\phi {\rm d}r$.
Column (7): $\log\Sigma_0 = \log\Upsilon_V^{\rm pop} + \log I_0$, the central surface mass density in units of $M_\odot$ pc^{-2}.
Column (8): $\log\rho_0 = \log\Upsilon_V^{\rm pop} + \log j_0$, the central volume density in units of $M_\odot$ pc^{-3}.
Column (9): $\log\Sigma_h = \log\Upsilon_V^{\rm pop} + \log I_h$, the surface mass density averaged over the half-light/effective radius R_h, in units of $M_\odot$ pc^{-2}.
Column (10): $\log\sigma_{p,0}$, the predicted line-of-sight velocity dispersion at the cluster center in units of km s^{-1}.
Column (11): $\log\nu_{\rm esc,0}$, the predicted central "escape" velocity in units of km s^{-1}, with which a star can move out from the center of a cluster, which is defined as $\nu_{\rm esc,0}^2/\sigma_0^2 = 2[W_0 + GM_{\rm tot}/r_t\sigma_0^2]$.
Column (12): $\log t_{r,h}$, the two-body relaxation time at the model-projected half-mass radius in units of years, estimated as $t_{r,h} = \frac{2.06\times10^6 yr}{\ln(0.4M_{\rm tot}/m_\star)}\frac{M_{\rm tot}^{1/2}R_h^{3/2}}{m_\star}$. Here, $m_\star$, the average stellar mass in a cluster is assumed to be $0.5M_\odot$ (see Mclaughlin et al. 2008, for the details)
Column (13): $\log f_0 \equiv \log[\rho_0/(2\pi\sigma_c^2)^{3/2}]$, the model's central phase-space density, in units of $M_\odot$ pc^{-3} (km s^{-1})$^{-3}$.

The uncertainties of these derived dynamical quantities were estimated from their variations in each model that yields χ^2 within 1 of the global minimum for a cluster, as above, and combined in quadrature with the uncertainties in $\Upsilon_V^{\rm pop}$.

3.3. *Comparison of Results in the F606W and F814W Filters*

Model fits for the same cluster observed in different filters were compared to check whether there were systematic errors or color dependencies in the fits. Figure 2 shows the comparison of some parameters derived from fits to the sample clusters in both F606W and F814W filters. The left panel shows the comparison of projected half-light radius, while the right panel shows the ratio of half-light to core radii, all of which are from Table 4. The uncertainties for the parameters were also given in Figure 2. It is evident that the results between the two ACS bands are in good agreement. In following analysis, the F606W model fits were used for all the sample GCs.

4. DISCUSSION

We combined the GC parameters derived here with those derived by King-model fits for clusters in the MW (Mclaughlin & van der Marel 2005) and M31 (Barmby et al. 2002, 2007, 2009; Huxor et al. 2011) to form a large sample to look into the correlations between the parameters. The ellipticities and galactocentric distances for the MW GCs are from Harris (1996) (2010 edition). For M31 GCs of Barmby et al. (2002) and Barmby et al. (2007) which were not observed in WFC F606W filter, the data of Space Telescope Imaging Spectrograph V-band or High Resolution Channel (HRC) F606W-band or HRC F555W-band or WFPC2 V-band are used, except for B082, of which the data of WFC F814W-band was used as Barmby et al. (2007) reported, since it was unsuccessfully fitted by King model in F606W filter. For clusters of Barmby et al. (2009) observed in WFPC2, the data of F439W- or F450W-band are used as Barmby et al. (2009) used, since these young clusters are dominated by blue stars and the measurements from the bluer filters are more preferred (see Barmby et al. 2009, for the details). Huxor et al. (2011) derived the structure parameters of 13 ECs based on V-band photometry (for INT) or g-band (for MegaCam) photometry. However, only metallicities of 4 ECs (HEC4, HEC5, HEC7 and HEC12) were determined by Mackey et al. (2006). We derived integrated cluster mass for the four ECs, using the V-band absolute magnitude obtained by Huxor et al. (2011) and a mass-to-light ratio determined with the same approach here (see §3.2 for details).

4.1. *Ellipticity Distribution*

As noted by Barmby et al. (2007), Larsen et al. (2001) listed several possible factors for the elongation of GCs: internal rotation, galaxy tides, cluster mergers, and "remnant elongation" from some clusters' former lives as dwarf galaxy nuclei. Cluster rotation is generally accepted to be a major factor for cluster flattening (Davoust & Prugniel 1990). However, van den Bergh & Morbey (1984) and van den Bergh (1996) presented that the brightest GCs in both the MW and M31 are most flattened, which can be explained by

---

[5] See http://www.ucolick.org/∼cnaw/sun.html.

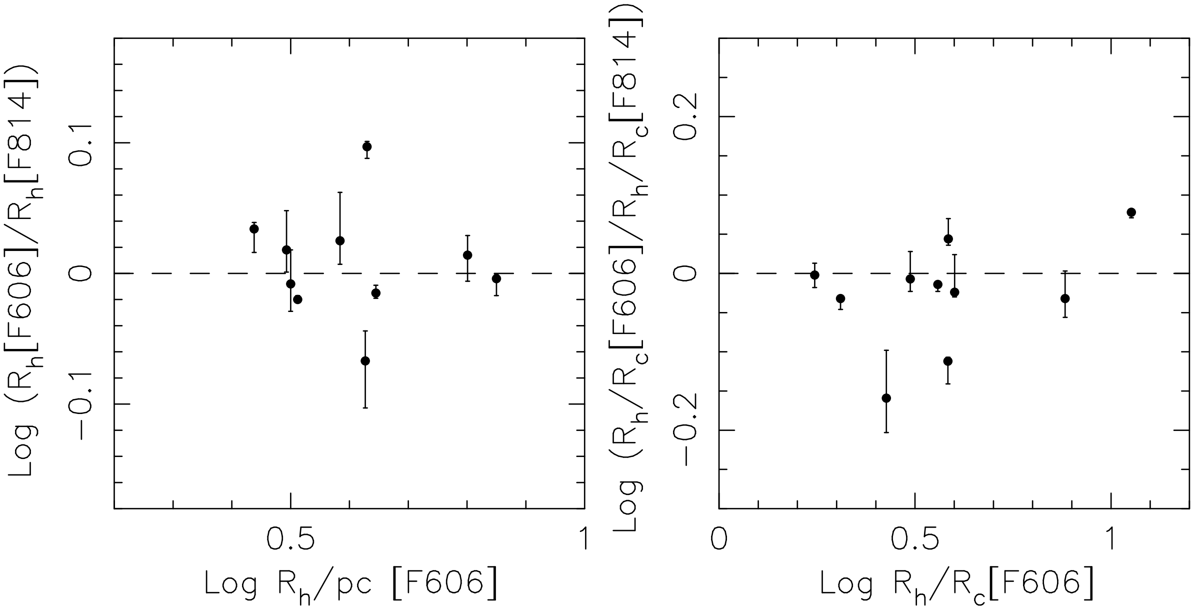

FIG. 2.— Comparison of parameters for model fits to the sample clusters in both F606W and F814W filters. *left* : projected half-light radius; *right* : ratio of half-light to core radii.

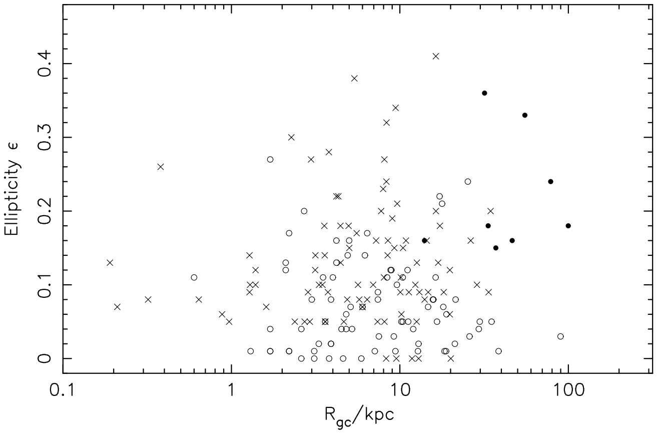

FIG. 3.— Ellipticity vs. galactocentric distance for GCs in M31 from Barmby et al. (2002, 2007) (crosses), in the outer halo of M31 from the present sample (filled circles) and the MW from Harris (1996) (2010 edition) (open circles).

the cluster mergers and "remnant elongation". In addition, as Harris et al. (2002) noted that dynamical models show that internal relaxation coupled to the external tides will in most situations drive a cluster toward a rounder shape over several relaxation times. Harris et al. (2002) presented that, the distributions of ellipticities for the M31 and NGC 5128 clusters and the old clusters in the Large Megallanic Cloud, are very similar, but different from the MW. With a large cluster sample, Barmby et al. (2007) also showed the distribution of ellipticities for clusters in the MW, M31 and NGC 5128, and found the distributions of ellipticities for M31 and NGC 5128 are not statistically different; both differ from the MW distribution in having few very round clusters. So, Barmby et al. (2007) concluded that there is no evidence that the overall galaxy environment is a major factor. Barmby et al. (2002) discussed about correlations of GC ellipticities with other properties in detail, and presented some explanations for these correlations combined with other authors' results (see Barmby et al. 2002, and references therein). In this paper, we show the distribution of ellipticity with galactocentric position for clusters in the MW and M31 in Figure 3, including the outer halo GCs in M31 from this study. A conclusion can be given that these outer halo GCs of M31 have larger ellipticities than most of GCs in M31 and the MW. These outer halo GCs lie at large projected radii than most sample clusters in Barmby et al. (2002, 2007), their large ellipticities may be due to galaxy tides coming from satellite dwarf galaxies of M31 or may be related to the apparently more vigorous accretion or merger history that M31 has experienced (e.g. Ibata et al. 2005, 2007; McConnachie et al. 2009; Bekki 2010; Hammer et al. 2010; Mackey et al. 2010; Huxor et al. 2011).

In order to show whether cluster ellipticities are caused by internal processes such as rotation or velocity anisotropy, Barmby et al. (2007) showed ellipticity as a function of luminosity and half-mass relaxation time for clusters in M31, NGC 5128 and the MW, since if it is true, relaxation through dynamical evolution should act to reduce any initial flattening (see Barmby et al. 2007, and references therein). These authors found a mild systematic decrease in ellipticity with increased luminosity, although considerable scatter, and no correlation of ellipticity with relaxation time is evident. So, Barmby et al. (2007) concluded that the observed distribution of GC ellipticity appears to be due to a number of factors. Figure 4 displays ellipticity as a function of model luminosity and half-mass relaxation time for clusters in the MW and M31, including the outer halo GCs in M31 studied here. It is evident that, when we add the data for the outer halo GCs in M31 obtained here, the conclusion of Barmby et al. (2007) will not evidently change, although the mild systematic decrease in ellipticity with increased luminosity nearly disappears. In addition, we think that the larger ellipticities of the outer halo GCs of M31 than most of GCs in M31 and the MW may be due to galaxy tides coming from satellite dwarf galaxies of M31 or may be related to the apparently more vigorous accretion or merger history that M31 has experienced.

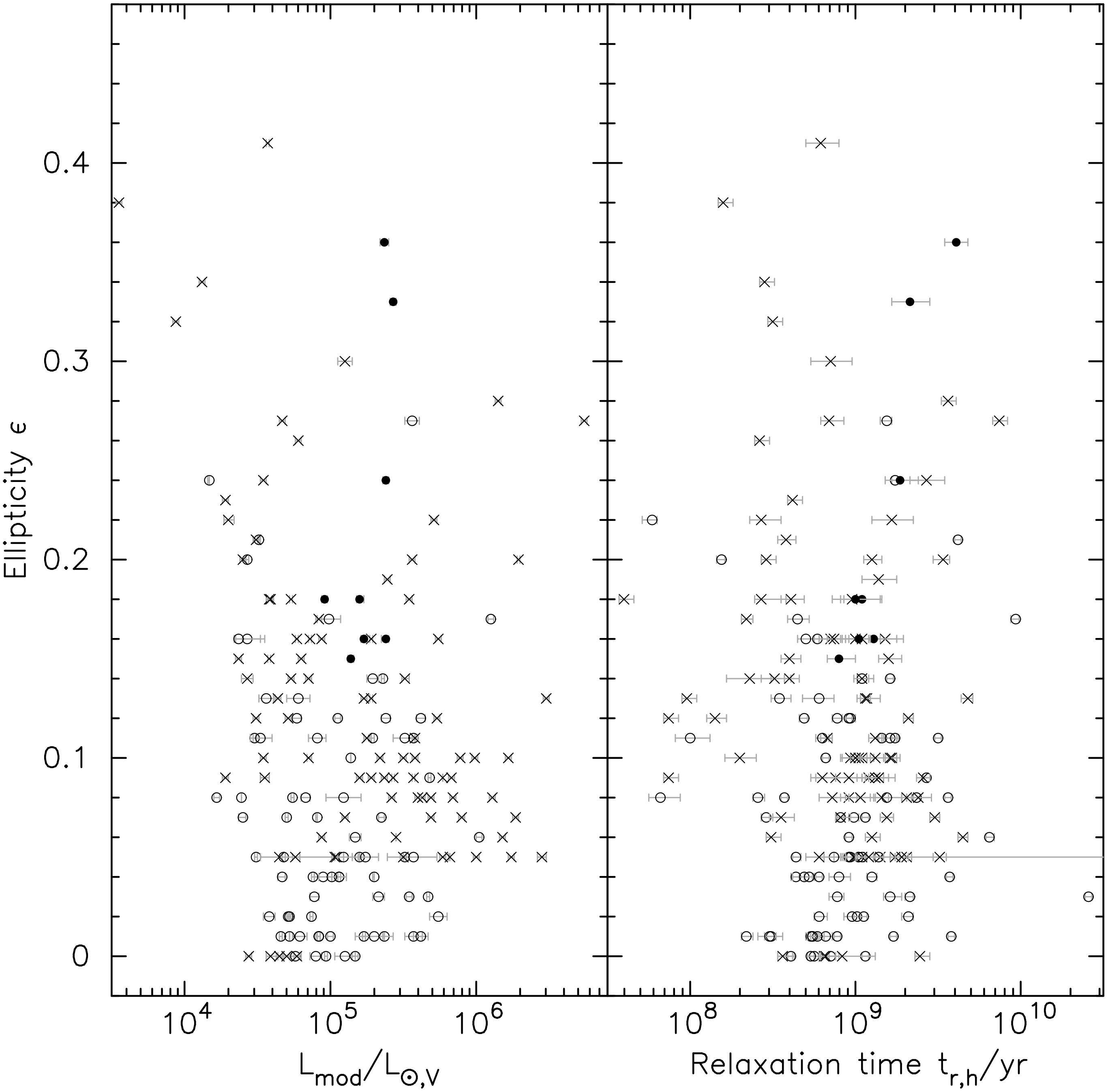

FIG. 4.— Ellipticity as a function of luminosity (*left*) and half-mass relaxation time (*right*) for GCs. Symbols are as in Fig. 3.

4.2. *Correlations with Position and Metallicity*

As Barmby et al. (2007) noted that, previous studies have shown that structures of the MW GCs are largely independent of galactocentric distances and metallicity, except for the correlation of half-light radius with galactocentric distances. Barmby et al. (2002) presented structural parameters as a function of galactocentric distance for clusters in M31 and the MW, and found that, there is no significant trend of c with $R_{\rm gc}$, both R_h and r_0 are correlated with $R_{\rm gc}$, and there is no clear correlation of $\mu_V(0)$ with $R_{\rm gc}$. The results of Barmby et al. (2002) are in agreement with ones obtained for GCs in the MW (e.g. Mclaughlin 2000) and NGC 5128 (e.g. Harris et al. 2002). Barmby et al. (2002) concluded that the correlations of R_h and r_0 with $R_{\rm gc}$ for GCs in both the MW and M31 are due to physical conditions at the time of cluster formation as suggested by van den Bergh et al. (1991) for MW GCs. Barmby et al. (2007) showed structural parameters as a function of galactocentric distance for GCs in the MW, the Magellanic Clouds and Fornax dwarf spheroidal, NGC 5128, and M31, and found similar results. In addition, Mackey & van den Bergh (2005) showed that there is a clear trend of increasing R_h with increasing $R_{\rm gc}$ for the Galactic GCs. We should notice that the galactocentric distances are true three-dimensional distances for Galactic GCs and projected radii for M31 clusters.

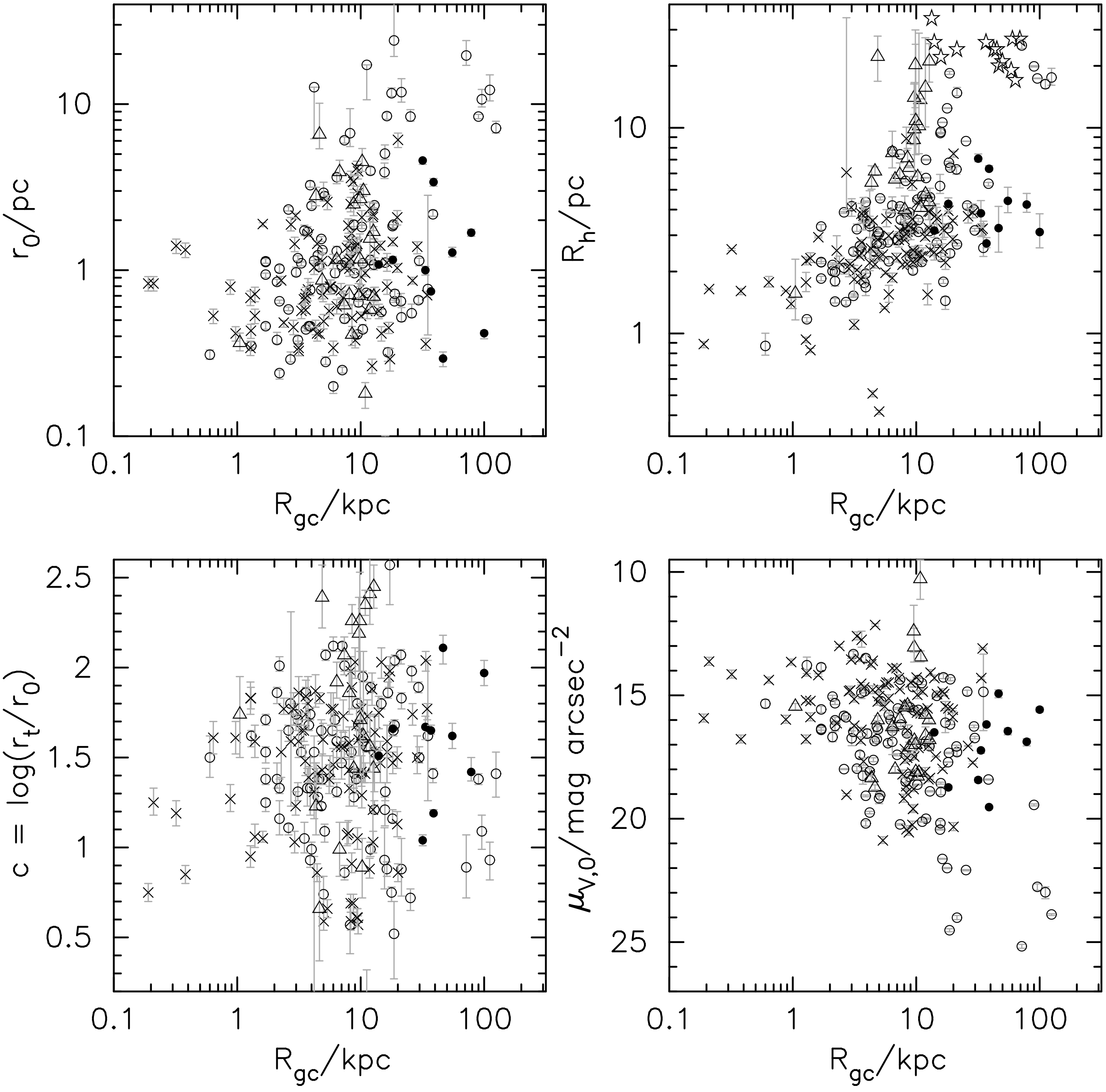

FIG. 5.— Structural parameters vs. galactocentric distance R_{gc}. The filled circles are GCs in the outer halo of M31 (this paper), the open circles are Galactic GCs (Mclaughlin & van der Marel 2005), the crosses are M31 GCs (Barmby et al. 2002, 2007), the open triangles are M31 young massive clusters (Barmby et al. 2009), the open stars are M31 ECs (Huxor et al. 2011).

Figure 5 shows structural parameters as a function of galactocentric distance R_{gc} for M31 outer halo GCs studied here, M31 young massive clusters (Barmby et al. 2009), MW globulars (Mclaughlin & van der Marel 2005), M31 globulars (Barmby et al. 2002, 2007) and M31 ECs (Huxor et al. 2011). It is evident that, when we add the data for the outer halo GCs in M31 obtained here, the conclusion of Barmby et al. (2002) will not change, with the exception that the galactocentric distances of M31 clusters can reach to 100 kpc which are as distant as the MW clusters. In addition, it is true that M31 young massive clusters have larger c and R_h than old GCs at the same galactocentric distances. For comparing with Huxor et al. (2011) (their Figure 9), we include the ECs of Huxor et al. (2011) in the upper-right panel of Figure 5, in which R_h is versus R_{gc}. It can be seen that, at large raddi (from 30 to 100 kpc) there are few GCs having R_h in the range from 8 to 15 pc, which is in agreement with the finding of Huxor et al. (2011).

Barmby et al. (2002) showed structural parameters as a function of [Fe/H] for clusters in M31 and the MW, and found that there is no correlation of metallicity with concentration c or central surface brightness $\mu_V(0)$, but there does appear to be a correlation with size, as measured by r_0 or R_h, i.e. r_0 or R_h deceases with increased metallicity. Harris et al. (2002) showed a different correlation of r_h with [Fe/H] for GCs in NGC 5128, where r_h is the half-mass radius, and reported that the correlation may be due to a selection effect because of a small sample. Barmby et al. (2007) showed structural parameters as a function of [Fe/H] for GCs in the MW, the Magellanic Clouds and Fornax dwarf spheroidal, NGC 5128, and M31, and found that, no correlation of c with [Fe/H] exists; a weak correlation of R_h with [Fe/H] is present: R_h deceases with increased metallicity, except for GCs in NGC 5128; there is a slight systematic increase of $\mu_{V,0}$ with [Fe/H].

Figure 6 plots structural parameters as a function of [Fe/H] for M31 outer halo GCs studied here, M31 young massive clusters (Barmby et al. 2009), MW globulars (Mclaughlin & van der Marel 2005), and M31 globulars (Barmby et al. 2002, 2007) and M31 ECs (Huxor et al. 2011). It is evident that, the outer halo GCs of M31 fall in the same regions of parameter spaces of clusters in M31 and the MW. In addition, the conclusions of Barmby et al. (2002) and Barmby et al. (2007) do not change when adding the young massive clusters of Barmby et al. (2009) and the outer halo GCs here. We also include four ECs of Huxor et al. (2011) in the upper-right panel of Figure 6. An evident feature is that these four ECs are all metal-poor and have large R_h.

Figure 7 plots structural parameters as a function of model mass $M_{\rm mod}$ for M31 outer halo GCs studied here, M31 young massive clusters (Barmby et al. 2009), MW globulars (Mclaughlin & van der Marel 2005), M31 globulars (Barmby et al. 2002, 2007) and M31 ECs (Huxor et al. 2011). The properties of clusters in M31 and the MW fall in the same regions of parameter spaces, with the exception that, on average, the young massive clusters have larger sizes and higher concentrations than older clusters of the same mass (see Barmby et al. 2009, for discussions in detail). We also include four ECs of Huxor et al. (2011) in the upper-right panel of Figure 7. Three ECs have intermediate masses as well as the outer halo GCs of M31 studied here, while one EC (HEC12) has very low mass ($\sim 2\times10^4$ M$_\odot$). Barmby et al. (2007) showed structural parameters as a function of model luminosity for GCs in M31, the MW, NGC 5128, the Magellanic Clouds, and the Fornax dSph, and found the properties of clusters in all six galaxies fall in the same regions of parameter spaces. The lower-right panel of Figure 7 shows one view of the fundamental plane, as defined by Mclaughlin (2000). Djorgovski (1995) found a pair of bivariate correlations in MW GC parameters which imply the existence of a "globular cluster fundamental plane", similar to that expected if the cores were virialized structures. Harris et al. (2002) found that the NGC 5128 GCs describe a relation between binding energy and luminosity that even tighter than in the MW, which occupy the same extremely narrow region of the parametric "fundamental plane" as do their MW counterparts.

5. SUMMARY

GCs in the outer halo of M31 have recently been discovered in many surveys. We selected ten GCs (15 kpc $\lesssim R_p \lesssim$ 100 kpc) which have been studied by Mackey et al. (2007) based on the *HST* observations used in this paper. We measured surface brightness profiles for them using the *HST* images of Mackey et al. (2007). Structural and dynamical parameters were derived by fitting the King model to the light profiles. We discussed the properties of the sample GCs here combined with GCs in the MW (Mclaughlin & van der Marel 2005) and clusters in M31 (Barmby et al. 2002, 2007, 2009). In general, the properties of the M31 and the Galactic clusters fall in the same regions of parameter spaces.

The outer halo GCs of M31, which lie at large projected radii, have larger ellipticities than most of GCs in M31 and the MW. Their large ellipticities may be due to galaxy tides coming from satellite dwarf galaxies of M31 or may be related to the apparently more vigorous accretion or merger history that M31 has experienced. However, this conclusion remains to be checked because of the sample limitation. RBC V4.0 provides 39 GCs and 87 GC candidates which lie at $R_p > 20$ kpc. With more and more *HST* observations, structural and dynamical parameters for these clusters can be measured, which will provide a larger sample for discussion on the halo GCs.

The strong correlation of E_b with model mass $M_{\rm mod}$ indicates a tight fundamental plane both for M31 and Galactic clusters, and no offset is apparent in the correlation between old and young clusters, especially including GCs in the outer halo of M31 studied here. This implies that some near-universal structural properties are present for clusters, regardless of their host environments, which is consistent with previous studies of Barmby et al. (2007, 2009).

We would like to thank Dr. McLaughlin for his help in finishing this paper. He provide us a table including some parameters being model-dependent function of W_0 or c. An anonymous referee is thanked for useful suggestions deriving from a careful and thorough reading of the original manuscript. This work was supported by the Chinese National Natural Science Foundation grant Nos. 10873016, and 10633020, and by the National Basic Research Program of China (973 Program) No. 2007CB815403.

REFERENCES

Barmby, P., Holland, S., & Huchra, J. P. 2002, AJ, 123, 1937
Barmby, P., Huchra, J., Brodie, J., et al. 2000, AJ, 119, 727
Barmby, P., McLaughlin, D. E., Harris, W. E., Harris, G. L. H., & Forbes, D. A. 2007, AJ, 133, 2764
Barmby, P., Perina, S., Bellazzini, M., et al. 2009, AJ, 138, 1667
Bekki, K. 2010, MNRAS, 401, L58
Bellazzini M., Ferraro F. R., & Ibata R. A. 2003, AJ, 125, 188
Brodie, J. P., & Strader, J. 2006, ARA&A, 44, 193
Brown, T. M., Ferguson, H. C., Smith, E., et al. 2005, AJ, 130, 1693
Bruzual, G., & Charlot, S. 2003, MNRAS, 344, 1000
Cardelli, J. A., Clayton, G. C., & Mathis, J. S. 1989, ApJ, 345, 245
Chabrier, G. 2003, PASP, 115, 763
Davoust, E., & Prugniel, P. 1990, A&A, 230, 67
Djorgovski, S. 1995, ApJ, 438, L29
Fan, Z., Ma, J., de Grijs, R., Yang, Y., & Zhou, X. 2006, MNRAS, 371, 1648
Federici, L., Bellazzini, M., Galleti, S., et al. 2007, A&A, 473, 429

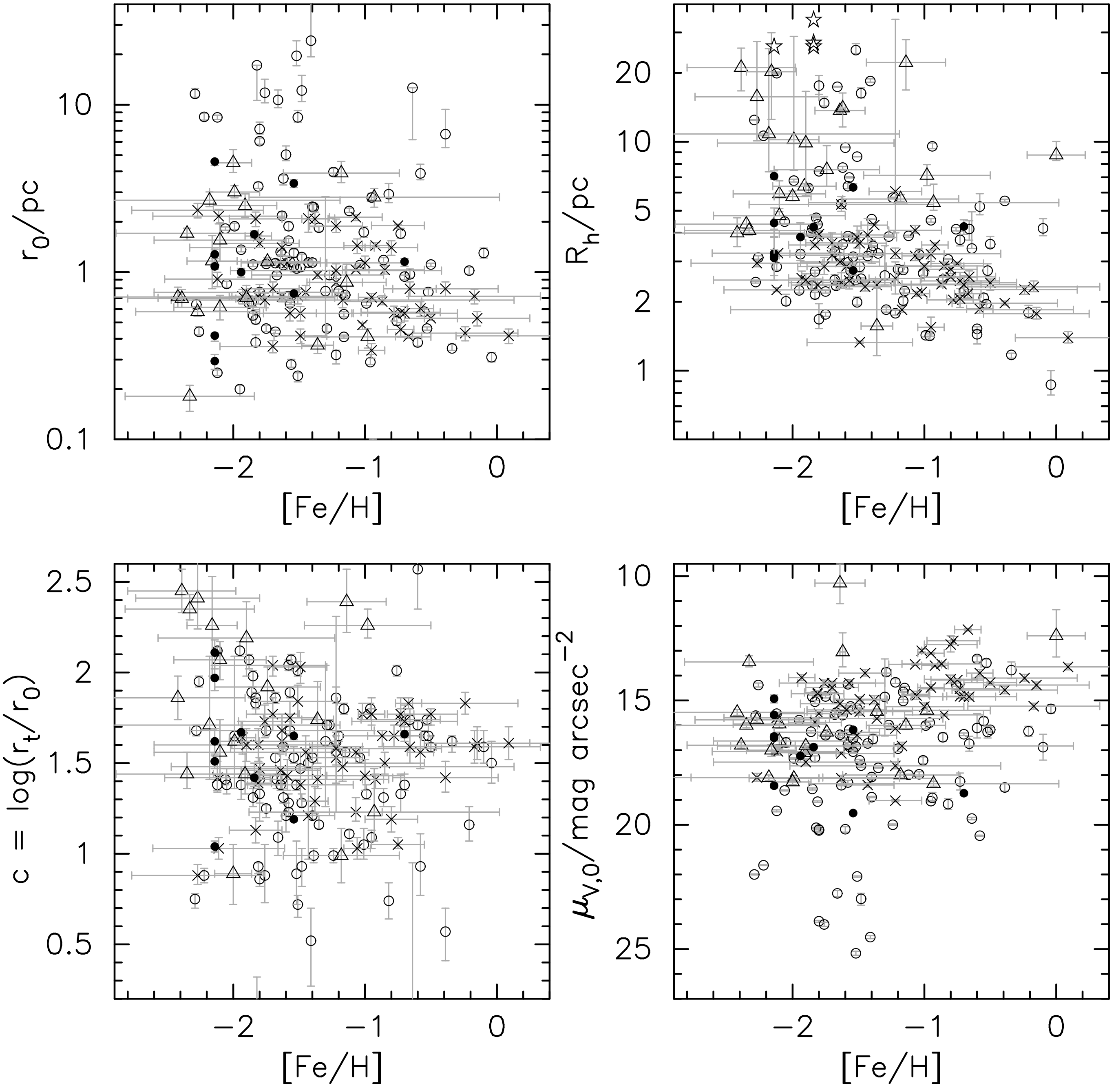

FIG. 6.— Structural parameters as a function of [Fe/H]. Symbols are as in Fig. 5.

Galleti, S., Bellazzini, M., Buzzoni, A., Federici, L., & Fusi Pecci, F. 2009, A&A, 508, 1285

Galleti, S., Bellazzini, M., Federici, L., Buzzoni, A., & Fusi Pecci, F. 2007, A&A, 471, 127

Galleti, S., Federici, L., Bellazzini, M., Buzzoni, A., & Fusi Pecci, F. 2006, A&A, 456, 985

Galleti, S., Federici, L., Bellazzini, M., Fusi Pecci, F., & Macrina, S. 2004, A&A, 426, 917

Grillmair, C. J., Ajhar, E. A., Faber, S. M., et al. 1996, AJ, 111, 2293

Hammer, F., Yang, Y. B., Wang, J. L., et al. 2010, ApJ, 725, 542

Harris, W. E. 1996, AJ, 112, 1487

Harris, W. E., Harris, G. L. H., Holland, S. T., & McLaughlin, D. E. 2002, AJ, 124, 1435

Holland, S., Côté, P., & Hesser, J. E. 1999, A&A, 348, 418

Huxor, A. P., Ferguson, A. M. N., Tanvir, N. R., et al. 2011, MNRAS, 414, 770

Huxor, A. P., Tanvir, N. R., Ferguson, A. M. N., et al. 2008, MNRAS, 385, 1989

Ibata, R., Chapman, S., Ferguson, A. M. N., et al. 2005, ApJ, 634, 287

Ibata, R., Martin, N. F., Irwin, M. et al. 2007, ApJ, 671, 1591

King, I. R. 1962, AJ, 67, 471

King, I. R. 1966, AJ, 71, 64

Larsen, S. S. 2001, AJ, 122, 1782

Larsen, S. S., Brodie, J. P., Sarajedini, A., & Huchra, J. P. 2002, AJ, 124, 2615

Ma, J. 2011, Res. Astron. Astrophys., 11, 524

Ma, J., de Grijs, R., Chen, D., et al. 2007, MNRAS, 376, 1621

Ma, J., Fan, Z., de Grijs, R., et al. 2009, AJ, 137, 4884

Ma, J., van den Bergh, S., Wu, H., et al. 2006, ApJ, 636, L93

Ma, J., Wang, S., Wu, Z., et al. 2011, AJ, 141, 86

Ma, J., Wang, S., Wu, Z., et al. 2012, AJ, 143, 29

Mackey, A. D., & Gilmore, G. F. 2003a, MNRAS, 338, 85

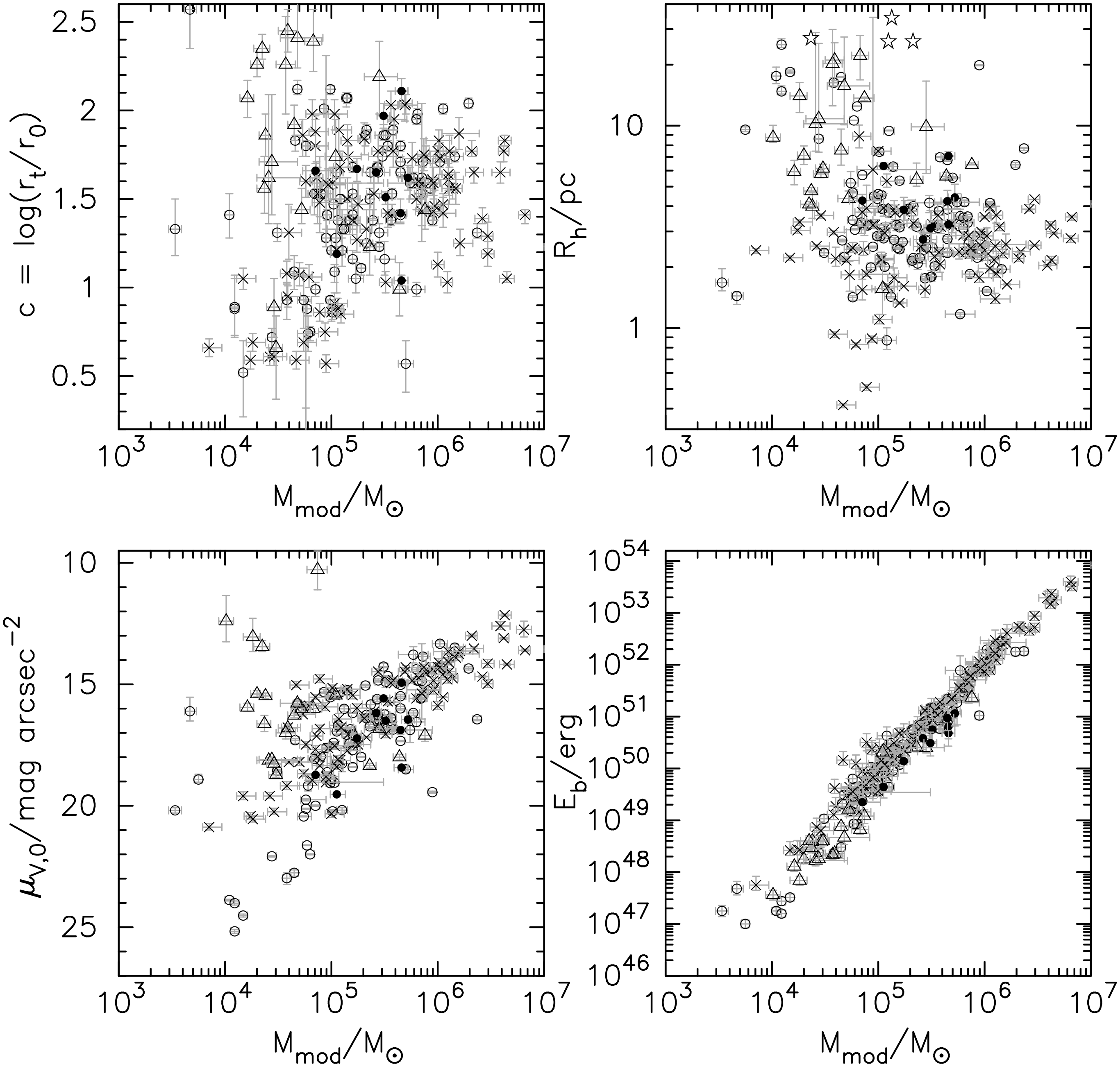

FIG. 7.— Structural parameters as a function of model mass $M_{\rm mod}$. Symbols are as in Fig. 5.

Mackey, A. D., & Gilmore, G. F. 2003b, MNRAS, 338, 120
Mackey, A. D., & Gilmore, G. F. 2003c, MNRAS, 340, 175
Mackey, A. D., & van den Bergh, S. 2005, MNRAS, 360, 631
Mackey, A. D., Huxor, A., Ferguson, A. M. N., et al. 2006, ApJ, 653, L105
Mackey, A. D., Huxor, A., Ferguson, A. M. N., et al. 2007, ApJ, 655, L85
Mackey, A. D., Huxor, A. P., Ferguson, A. M. N., et al. 2010, ApJ, 717, L11
McLaughlin, D. E. 2000, ApJ, 539, 618
McLaughlin, D. E.,Barmby, P., Harris, W. E., Forbes, D. A., & Harris, G. L. H. 2008, MNRAS, 384, 563
McLaughlin, D. E., & van der Marel, R. P. 2005, ApJS, 161, 304
Macri, L. M. 2001, ApJ, 549, 721
Martin, N. F., Ibata, R. A., Irwin, M. J., et al. 2006, MNRAS, 371, 1983
Martini, P., & Ho, L. C. 2004, ApJ, 610, 233
McConnachie, A. W., Irwin, M. J., Ibata, R. A. et al. 2009, Natur, 461, 66
Perina, S., Barmby, P., Beasley, M. A., et al. 2009, A&A, 494, 933
Perina, S., Cohen, J. G., Barmby, P., et al. 2010, A&A, 511, A23
Perrett, K. M., Bridges, T. J., Hanes, D. A., et al. 2002, AJ, 123, 2490
Puzia, T. H., Perrett, K. M., & Bridges, T. J. 2005, A&A, 434, 909
Reed, L. G., Harris, G. L. H., & Harris, W. E. 1992, AJ, 103, 824
Richardson, J. C., Ferguson, A. M. N., Mackey, A. D., et al. 2009, MNRAS, 396, 1842
Sérsic, J.-L. 1968, Atlas de Galaxias Australes (Cordoba: Obs. Astronomico)
Sirianni, M., Jee, M. J., Benítez, N., et al. 2005, PASP, 117, 1049
Stanek K. Z., & Garnavich, P. M. 1998, ApJ, 503, 131
Strader, J., Smith, G. H., Larsen, S., et al. 2009, AJ, 138, 547
Trager, S. C., Djorgovski, S., & King, I. R. 1993, in structure and Dynamics of Globular Clusters, ASP Conf.Series 50, ed. S.G.Djorgovski and G.Meylan (San Francisco: A.S.P.), 373
Trager, S. C., King, I. R., & Djorgovski, S. 1995, AJ, 109, 218
van den Bergh, S. 1996, Observatory, 116, 103

van den Bergh, S., & Morbey, C. L. 1984, ApJ, 283, 598
van den Bergh, S., Morbey, C., & Pazder, J. 1991, ApJ, 375, 594
Wang, S., Fan, Z., Ma, J., de Grijs, R., & Zhou, X. 2010, AJ, 139, 1438
Wilson, C. P. 1975, AJ, 80, 175

TABLE 1
Integrated Measurements for the 10 GCs in the M31 Halo.

Name	ϵ^a(F606W)	ϵ^a(F814W)	θ^b(F606W) (deg E of N)	θ^b(F814W) (deg E of N)	V (VEGAMAG)	I (VEGAMAG)	$R_{\rm gc}$ (kpc)	$(m-M)_0$	$E(B-V)$	[Fe/H]
GC1	0.16 ± 0.09	0.23 ± 0.14	-91 ± 60	-86 ± 49	16.050	15.070	46.4	24.41	0.09	−2.14
GC2	0.18 ± 0.07	0.21 ± 0.09	-134 ± 36	-132 ± 38	16.980	16.040	33.4	24.32	0.08	−1.94
GC3	0.36 ± 0.25	...	-126 ± 49	...	16.310	15.360	31.8	24.37	0.11	−2.14
GC4	0.33 ± 0.20	0.30 ± 0.21	-139 ± 61	-147 ± 57	15.760	14.680	55.2	24.35	0.09	−2.14
GC5	0.24 ± 0.16	0.15 ± 0.08	-165 ± 69	-165 ± 49	16.090	15.010	78.5	24.45	0.08	−1.84
GC6[c]	0.16 ± 0.12	0.32 ± 0.26	-123 ± 68	-116 ± 60	16.590	15.460	14.0	24.49	0.09	−2.14
GC7	...	...	...	...	18.270	17.070	18.2	24.13	0.06	−0.70
GC8	0.15 ± 0.08	0.22 ± 0.15	-183 ± 43	-137 ± 55	16.720	15.680	37.1	24.43	0.09	−1.54
GC9	...	0.35 ± 0.16	...	-135 ± 43	17.780	16.710	38.9	24.22	0.15	−1.54
GC10	0.18 ± 0.13	0.13 ± 0.05	-160 ± 49	-152 ± 37	16.500	15.590	99.9	24.42	0.09	−2.14

[a] $\epsilon = 1 - b/a$, while a and b are the lengths of the semimajor and semiminor axes, respectively.

[b] Position angle (P.A.)is measured in degrees anticlockwise from North.

[c] GC6 is called B298 in RBC V4.0.

TABLE 2
The 20 F606W, F814W Intensity Profiles of the 10 GCs in the M31 Halo.

Name (1)	Detector (2)	Filter (3)	R (arcsec) (4)	I $L_\odot$ pc^{-2} (5)	Uncertainty $L_\odot$ pc^{-2} (6)	Flag (7)
GC1	WFC	F606W	0.0260	31738.412	202.312	OK
GC1	WFC	F606W	0.0287	31294.604	223.745	DEP
GC1	WFC	F606W	0.0315	30807.689	243.173	DEP
GC1	WFC	F606W	0.0347	30277.402	263.883	DEP
GC1	WFC	F606W	0.0381	29710.863	294.703	DEP
GC1	WFC	F606W	0.0420	29090.574	324.043	DEP
GC1	WFC	F606W	0.0461	28412.213	351.340	DEP
GC1	WFC	F606W	0.0508	27656.385	368.209	DEP
GC1	WFC	F606W	0.0558	26734.781	357.023	OK
GC1	WFC	F606W	0.0614	25634.490	362.977	DEP
GC1	WFC	F606W	0.0676	24403.732	376.725	DEP

Note. — Table 2 is published in its entirety in the electronic edition of the Journal. Only a small portion is shown here, for guidance regarding its form and content. See text for description of the FLAG column.

TABLE 3
BASIC PARAMETERS OF THE 20 PROFILES OF THE 10 GCS IN THE M31 HALO.

Name (1)	Detector (2)	$(V-\mathrm{F606W})_0$ (mag) (3)	N_{pts} (4)	Model (5)	χ^2_{min} (6)	I_{bkg} $L_\odot$ pc^{-2} (7)	W_0 (8)	c (9)	μ_0 (mag arcsec^{-2}) (10)	$\log r_0$ (arcsec) (11)	$\log r_0$ (pc) (12)
GC1	WFC/F606	0.189 ± 0.050	57	K66	3401.76	0.20 ± 0.08	$8.96^{+0.27}_{-0.31}$	$2.11^{+0.07}_{-0.09}$	$14.73^{+0.18}_{-0.13}$	$-1.100^{+0.039}_{-0.049}$	$-0.532^{+0.039}_{-0.049}$
	WFC/F814		56		2083.76	0.00 ± 0.13	$8.72^{+0.27}_{-0.32}$	$2.04^{+0.07}_{-0.09}$	$14.35^{+0.20}_{-0.17}$	$-1.000^{+0.032}_{-0.048}$	$-0.432^{+0.032}_{-0.048}$
GC2	WFC/F606	0.183 ± 0.050	53	K66	686.35	0.20 ± 0.12	$7.49^{+0.20}_{-0.22}$	$1.67^{+0.06}_{-0.07}$	$17.05^{+0.11}_{-0.06}$	$-0.550^{+0.022}_{-0.030}$	$0.000^{+0.022}_{-0.030}$
	WFC/F814		53		743.06	0.10 ± 0.15	$7.58^{+0.35}_{-0.21}$	$1.70^{+0.11}_{-0.06}$	$16.24^{+0.09}_{-0.09}$	$-0.600^{+0.034}_{-0.043}$	$-0.050^{+0.034}_{-0.043}$
GC3	WFC/F606	0.172 ± 0.050	30	K66	262.8	0.70 ± 0.12	$5.06^{+0.16}_{-0.14}$	$1.04^{+0.03}_{-0.03}$	$18.25^{+0.08}_{-0.09}$	$0.100^{+0.007}_{-0.023}$	$0.660^{+0.007}_{-0.023}$
	WFC/F814		29		195.46	0.80 ± 0.18	$5.09^{+0.18}_{-0.22}$	$1.05^{+0.04}_{-0.05}$	$17.63^{+0.12}_{-0.09}$	$0.100^{+0.012}_{-0.012}$	$0.660^{+0.012}_{-0.012}$
GC4	WFC/F606	0.216 ± 0.050	57	K66	1378.26	0.60 ± 0.16	$7.31^{+0.21}_{-0.24}$	$1.62^{+0.07}_{-0.07}$	$16.24^{+0.14}_{-0.12}$	$-0.450^{+0.031}_{-0.027}$	$0.106^{+0.031}_{-0.027}$
	WFC/F814		57		935.37	0.90 ± 0.34	$7.37^{+0.23}_{-0.23}$	$1.64^{+0.07}_{-0.07}$	$15.62^{+0.13}_{-0.14}$	$-0.450^{+0.025}_{-0.030}$	$0.106^{+0.025}_{-0.030}$
GC5	WFC/F606	0.222 ± 0.050	49	K66	687.47	1.00 ± 0.31	$6.62^{+0.28}_{-0.20}$	$1.42^{+0.08}_{-0.05}$	$16.65^{+0.16}_{-0.11}$	$-0.350^{+0.020}_{-0.022}$	$0.226^{+0.020}_{-0.022}$
	WFC/F814		54		2066.58	0.40 ± 1.03	$7.43^{+0.27}_{-0.33}$	$1.66^{+0.08}_{-0.10}$	$15.87^{+0.16}_{-0.09}$	$-0.450^{+0.029}_{-0.060}$	$0.126^{+0.029}_{-0.060}$
GC6	WFC/F606	0.230 ± 0.050	54	K66	477.9	0.60 ± 0.11	$6.95^{+0.11}_{-0.13}$	$1.51^{+0.03}_{-0.04}$	$16.27^{+0.04}_{-0.03}$	$-0.550^{+0.018}_{-0.017}$	$0.034^{+0.018}_{-0.017}$
	WFC/F814		54		404.46	0.90 ± 0.25	$6.98^{+0.22}_{-0.26}$	$1.52^{+0.07}_{-0.08}$	$15.67^{+0.09}_{-0.12}$	$-0.550^{+0.015}_{-0.026}$	$0.034^{+0.015}_{-0.026}$
GC7	WFC/F606	0.261 ± 0.050	34	K66	196.86	0.10 ± 0.00	$7.43^{+0.11}_{-0.13}$	$1.66^{+0.04}_{-0.04}$	$18.46^{+0.09}_{-0.06}$	$-0.450^{+0.020}_{-0.027}$	$0.062^{+0.020}_{-0.027}$
	WFC/F814		34		229.16	0.20 ± 0.00	$7.22^{+0.14}_{-0.11}$	$1.59^{+0.04}_{-0.03}$	$17.18^{+0.08}_{-0.05}$	$-0.500^{+0.021}_{-0.049}$	$0.012^{+0.021}_{-0.049}$
GC8	WFC/F606	0.205 ± 0.050	48	K66	170.88	0.60 ± 0.15	$7.40^{+0.08}_{-0.07}$	$1.65^{+0.03}_{-0.02}$	$15.98^{+0.04}_{-0.03}$	$-0.700^{+0.006}_{-0.013}$	$-0.128^{+0.006}_{-0.013}$
	WFC/F814		47		186.59	0.70 ± 0.19	$7.82^{+0.09}_{-0.12}$	$1.78^{+0.03}_{-0.04}$	$14.99^{+0.05}_{-0.06}$	$-0.850^{+0.016}_{-0.014}$	$-0.278^{+0.016}_{-0.014}$
GC9	WFC/F606	0.189 ± 0.050	33	K66	321.09	0.40 ± 0.03	$5.75^{+0.07}_{-0.06}$	$1.19^{+0.02}_{-0.01}$	$19.33^{+0.03}_{-0.02}$	$0.000^{+0.022}_{-0.024}$	$0.530^{+0.022}_{-0.024}$
	WFC/F814		32		82.88	-0.30 ± 0.09	$6.02^{+0.20}_{-0.16}$	$1.26^{+0.05}_{-0.04}$	$18.63^{+0.13}_{-0.07}$	$-0.050^{+0.017}_{-0.015}$	$0.480^{+0.017}_{-0.015}$
GC10	WFC/F606	0.169 ± 0.050	54	K66	1433.16	1.20 ± 0.14	$8.45^{+0.25}_{-0.24}$	$1.97^{+0.07}_{-0.07}$	$15.42^{+0.10}_{-0.09}$	$-0.950^{+0.015}_{-0.033}$	$-0.380^{+0.015}_{-0.033}$
	WFC/F814		54		1280.34	1.10 ± 0.17	$8.54^{+0.30}_{-0.25}$	$1.99^{+0.08}_{-0.07}$	$14.77^{+0.11}_{-0.09}$	$-1.000^{+0.021}_{-0.039}$	$-0.430^{+0.021}_{-0.039}$

TABLE 4

Derived Structural and Photometric Parameters from the 20 Profiles of the 10 GCs in the M31 Halo.

Name	Detector	Model	$\log r_{\rm tid}$	$\log R_c$	$\log R_h$	$\log R_h/R_c$	$\log I_0$	$\log j_0$	$\log L_V$	$V_{\rm tot}$	$\log I_h$	$< \mu_V >_h$
			(pc)	(pc)	(pc)		$L_{\odot,V}$ pc^{-2}	$L_{\odot,V}$ pc^{-3}	$L_{\odot,V}$	(mag)	$L_{\odot,V}$ pc^{-2}	(mag arcsec^{-2})
(1)	(2)	(3)	(4)	(5)	(6)	(7)	(8)	(9)	(10)	(11)	(12)	(14)
GC1	WFC/F606	K66	$1.58^{+0.07}_{-0.08}$	$-0.540^{+0.037}_{-0.048}$	$0.512^{+0.106}_{-0.117}$	$1.052^{+0.154}_{-0.154}$	$4.59^{+0.06}_{-0.07}$	$4.83^{+0.10}_{-0.11}$	$5.38^{+0.02}_{-0.03}$	$15.79^{+0.07}_{-0.06}$	$3.56^{+0.21}_{-0.19}$	$17.50^{+0.47}_{-0.52}$
	WFC/F814		$1.61^{+0.07}_{-0.09}$	$-0.441^{+0.030}_{-0.047}$	$0.532^{+0.109}_{-0.117}$	$0.974^{+0.156}_{-0.147}$		$4.73^{+0.10}_{-0.10}$			$3.52^{+0.21}_{-0.19}$	$17.61^{+0.48}_{-0.52}$
GC2	WFC/F606	K66	$1.67^{+0.06}_{-0.07}$	$-0.017^{+0.020}_{-0.028}$	$0.584^{+0.062}_{-0.069}$	$0.601^{+0.091}_{-0.089}$	$3.67^{+0.03}_{-0.05}$	$3.38^{+0.06}_{-0.07}$	$4.96^{+0.02}_{-0.02}$	$16.74^{+0.05}_{-0.05}$	$3.00^{+0.12}_{-0.10}$	$18.91^{+0.26}_{-0.29}$
	WFC/F814		$1.65^{+0.11}_{-0.06}$	$-0.066^{+0.032}_{-0.041}$	$0.559^{+0.099}_{-0.051}$	$0.625^{+0.139}_{-0.083}$		$3.43^{+0.07}_{-0.08}$			$3.05^{+0.08}_{-0.18}$	$18.78^{+0.44}_{-0.20}$
GC3	WFC/F606	K66	$1.70^{+0.03}_{-0.03}$	$0.607^{+0.004}_{-0.019}$	$0.850^{+0.023}_{-0.015}$	$0.244^{+0.043}_{-0.019}$	$3.19^{+0.04}_{-0.04}$	$2.28^{+0.06}_{-0.04}$	$5.37^{+0.03}_{-0.03}$	$15.77^{+0.08}_{-0.08}$	$2.87^{+0.00}_{-0.01}$	$19.21^{+0.03}_{0.00}$
	WFC/F814		$1.71^{+0.04}_{-0.04}$	$0.608^{+0.007}_{-0.008}$	$0.854^{+0.020}_{-0.028}$	$0.246^{+0.028}_{-0.035}$		$2.28^{+0.05}_{-0.05}$			$2.87^{+0.02}_{-0.01}$	$19.23^{+0.02}_{-0.06}$
GC4	WFC/F606	K66	$1.73^{+0.07}_{-0.07}$	$0.087^{+0.028}_{-0.025}$	$0.645^{+0.066}_{-0.058}$	$0.558^{+0.091}_{-0.086}$	$3.98^{+0.05}_{-0.06}$	$3.59^{+0.08}_{-0.09}$	$5.43^{+0.02}_{-0.02}$	$15.60^{+0.06}_{-0.05}$	$3.34^{+0.09}_{-0.11}$	$18.04^{+0.28}_{-0.23}$
	WFC/F814		$1.74^{+0.07}_{-0.07}$	$0.088^{+0.023}_{-0.028}$	$0.660^{+0.060}_{-0.054}$	$0.572^{+0.087}_{-0.077}$		$3.59^{+0.08}_{-0.08}$			$3.31^{+0.09}_{-0.10}$	$18.12^{+0.25}_{-0.21}$
GC5	WFC/F606	K66	$1.64^{+0.08}_{-0.05}$	$0.200^{+0.018}_{-0.018}$	$0.627^{+0.054}_{-0.038}$	$0.427^{+0.073}_{-0.056}$	$3.81^{+0.05}_{-0.07}$	$3.31^{+0.07}_{-0.09}$	$5.38^{+0.02}_{-0.02}$	$15.84^{+0.05}_{-0.05}$	$3.32^{+0.06}_{-0.09}$	$18.09^{+0.22}_{-0.14}$
	WFC/F814		$1.78^{+0.09}_{-0.10}$	$0.108^{+0.025}_{-0.057}$	$0.694^{+0.077}_{-0.074}$	$0.586^{+0.134}_{-0.100}$		$3.40^{+0.11}_{-0.09}$			$3.19^{+0.13}_{-0.13}$	$18.43^{+0.33}_{-0.32}$
GC6	WFC/F606	K66	$1.55^{+0.03}_{-0.04}$	$0.012^{+0.017}_{-0.016}$	$0.500^{+0.030}_{-0.033}$	$0.488^{+0.045}_{-0.050}$	$3.96^{+0.02}_{-0.02}$	$3.64^{+0.04}_{-0.04}$	$5.23^{+0.02}_{-0.02}$	$16.26^{+0.05}_{-0.05}$	$3.43^{+0.05}_{-0.04}$	$17.83^{+0.10}_{-0.12}$
	WFC/F814		$1.55^{+0.07}_{-0.07}$	$0.012^{+0.012}_{-0.024}$	$0.508^{+0.056}_{-0.054}$	$0.495^{+0.080}_{-0.066}$		$3.64^{+0.05}_{-0.04}$			$3.41^{+0.09}_{-0.09}$	$17.87^{+0.23}_{-0.22}$
GC7	WFC/F606	K66	$1.72^{+0.04}_{-0.04}$	$0.044^{+0.019}_{-0.026}$	$0.630^{+0.029}_{-0.035}$	$0.585^{+0.056}_{-0.054}$	$3.07^{+0.03}_{-0.04}$	$2.72^{+0.06}_{-0.06}$	$4.46^{+0.03}_{-0.03}$	$17.80^{+0.06}_{-0.06}$	$2.40^{+0.04}_{-0.03}$	$20.39^{+0.08}_{-0.11}$
	WFC/F814		$1.60^{+0.04}_{-0.03}$	$-0.008^{+0.020}_{-0.048}$	$0.533^{+0.033}_{-0.026}$	$0.541^{+0.082}_{-0.046}$		$2.78^{+0.08}_{-0.06}$			$2.60^{+0.03}_{-0.04}$	$19.91^{+0.10}_{-0.07}$
GC8	WFC/F606	K66	$1.52^{+0.03}_{-0.02}$	$-0.146^{+0.005}_{-0.013}$	$0.438^{+0.028}_{-0.021}$	$0.584^{+0.041}_{-0.026}$	$4.09^{+0.02}_{-0.03}$	$3.93^{+0.04}_{-0.03}$	$5.14^{+0.02}_{-0.02}$	$16.40^{+0.05}_{-0.05}$	$3.47^{+0.02}_{-0.04}$	$17.73^{+0.09}_{-0.05}$
	WFC/F814		$1.50^{+0.03}_{-0.04}$	$-0.293^{+0.015}_{-0.013}$	$0.404^{+0.033}_{-0.039}$	$0.696^{+0.046}_{-0.055}$		$4.07^{+0.04}_{-0.04}$			$3.54^{+0.06}_{-0.05}$	$17.55^{+0.11}_{-0.15}$
GC9	WFC/F606	K66	$1.72^{+0.02}_{-0.01}$	$0.491^{+0.021}_{-0.023}$	$0.801^{+0.015}_{-0.008}$	$0.310^{+0.038}_{-0.028}$	$2.75^{+0.02}_{-0.02}$	$1.96^{+0.05}_{-0.04}$	$4.77^{+0.02}_{-0.02}$	$17.12^{+0.05}_{-0.06}$	$2.37^{+-0.01}_{-0.01}$	$20.47^{+0.02}_{0.01}$
	WFC/F814		$1.74^{+0.05}_{-0.04}$	$0.446^{+0.015}_{-0.012}$	$0.787^{+0.030}_{-0.028}$	$0.342^{+0.042}_{-0.042}$		$2.00^{+0.03}_{-0.04}$			$2.40^{+0.03}_{-0.04}$	$20.40^{+0.09}_{-0.09}$
GC10	WFC/F606	K66	$1.59^{+0.07}_{-0.07}$	$-0.391^{+0.014}_{-0.032}$	$0.493^{+0.089}_{-0.077}$	$0.883^{+0.121}_{-0.090}$	$4.33^{+0.04}_{-0.04}$	$4.41^{+0.07}_{-0.06}$	$5.20^{+0.03}_{-0.02}$	$16.24^{+0.06}_{-0.07}$	$3.42^{+0.13}_{-0.15}$	$17.85^{+0.38}_{-0.33}$
	WFC/F814		$1.56^{+0.09}_{-0.07}$	$-0.440^{+0.020}_{-0.037}$	$0.475^{+0.119}_{-0.094}$	$0.915^{+0.156}_{-0.114}$		$4.46^{+0.08}_{-0.06}$			$3.46^{+0.17}_{-0.21}$	$17.76^{+0.53}_{-0.41}$

TABLE 5

Derived Dynamical Parameters from the 20 Profiles of the 10 GCs in the M31 Halo.

Name (1)	Detector (2)	$\Upsilon_V^{\rm pop}$ $M_\odot$ $L_{\odot,V}^{-1}$ (3)	Model (4)	$\log M_{\rm tot}$ $M_\odot$ (5)	$\log E_b$ (erg) (6)	$\log \Sigma_0$ $M_\odot$ pc^{-2} (7)	$\log \rho_0$ $M_\odot$ pc^{-3} (8)	$\log \Sigma_h$ $M_\odot$ pc^{-2} (9)	$\log \sigma_{p,0}$ (km s^{-1}) (10)	$\log \nu_{\rm esc,0}$ (km s^{-1}) (11)	$\log t_{r,h}$ yr (12)	$\log f_0$ $M_\odot$ (pc km s^{-1})$^{-3}$) (13)
GC1	WFC/F606	$1.918^{+0.244}_{-0.237}$	K66	$5.66^{+0.06}_{-0.06}$	$50.68^{+0.21}_{-0.25}$	$4.88^{+0.08}_{-0.09}$	$5.11^{+0.12}_{-0.13}$	$3.84^{+0.20}_{-0.22}$	$0.906^{+0.026}_{-0.034}$	$1.539^{+0.028}_{-0.038}$	$9.11^{+0.18}_{-0.20}$	$1.183^{+0.098}_{-0.065}$
	WFC/F814	$1.918^{+0.244}_{-0.237}$			$50.93^{+0.21}_{-0.26}$	$4.88^{+0.08}_{-0.09}$	$5.01^{+0.12}_{-0.12}$	$3.80^{+0.20}_{-0.21}$	$0.956^{+0.026}_{-0.036}$	$1.584^{+0.028}_{-0.041}$	$9.14^{+0.18}_{-0.19}$	$0.933^{+0.096}_{-0.050}$
GC2	WFC/F606	$1.889^{+0.257}_{-0.226}$	K66	$5.24^{+0.06}_{-0.06}$	$50.14^{+0.22}_{-0.23}$	$3.94^{+0.06}_{-0.07}$	$3.66^{+0.08}_{-0.09}$	$3.27^{+0.12}_{-0.13}$	$0.704^{+0.028}_{-0.031}$	$1.305^{+0.028}_{-0.034}$	$9.04^{+0.12}_{-0.13}$	$0.325^{+0.064}_{-0.040}$
	WFC/F814	$1.889^{+0.257}_{-0.226}$			$50.00^{+0.22}_{-0.22}$	$3.94^{+0.06}_{-0.07}$	$3.71^{+0.09}_{-0.10}$	$3.32^{+0.18}_{-0.10}$	$0.679^{+0.028}_{-0.029}$	$1.282^{+0.028}_{-0.031}$	$9.00^{+0.17}_{-0.10}$	$0.449^{+0.094}_{-0.064}$
GC3	WFC/F606	$1.918^{+0.244}_{-0.237}$	K66	$5.66^{+0.06}_{-0.07}$	$50.81^{+0.21}_{-0.24}$	$3.47^{+0.07}_{-0.07}$	$2.56^{+0.08}_{-0.07}$	$3.16^{+0.05}_{-0.06}$	$0.784^{+0.028}_{-0.034}$	$1.331^{+0.030}_{-0.035}$	$9.61^{+0.07}_{-0.07}$	$-1.041^{+0.040}_{-0.030}$
	WFC/F814	$1.918^{+0.244}_{-0.237}$			$50.82^{+0.22}_{-0.24}$	$3.47^{+0.07}_{-0.07}$	$2.56^{+0.07}_{-0.07}$	$3.15^{+0.05}_{-0.06}$	$0.784^{+0.031}_{-0.033}$	$1.332^{+0.033}_{-0.035}$	$9.62^{+0.07}_{-0.08}$	$-1.042^{+0.026}_{-0.029}$
GC4	WFC/F606	$1.918^{+0.244}_{-0.237}$	K66	$5.72^{+0.06}_{-0.06}$	$51.06^{+0.22}_{-0.24}$	$4.26^{+0.07}_{-0.08}$	$3.87^{+0.09}_{-0.10}$	$3.63^{+0.12}_{-0.11}$	$0.914^{+0.029}_{-0.032}$	$1.511^{+0.031}_{-0.035}$	$9.33^{+0.12}_{-0.11}$	$-0.096^{+0.048}_{-0.054}$
	WFC/F814	$1.918^{+0.244}_{-0.237}$			$51.07^{+0.21}_{-0.24}$	$4.26^{+0.07}_{-0.08}$	$3.87^{+0.09}_{-0.10}$	$3.60^{+0.11}_{-0.10}$	$0.914^{+0.028}_{-0.033}$	$1.513^{+0.031}_{-0.036}$	$9.35^{+0.11}_{-0.11}$	$-0.097^{+0.054}_{-0.043}$
GC5	WFC/F606	$1.881^{+0.275}_{-0.223}$	K66	$5.65^{+0.06}_{-0.06}$	$50.97^{+0.25}_{-0.24}$	$4.09^{+0.08}_{-0.09}$	$3.58^{+0.09}_{-0.10}$	$3.60^{+0.11}_{-0.08}$	$0.885^{+0.033}_{-0.037}$	$1.467^{+0.036}_{-0.040}$	$9.27^{+0.11}_{-0.09}$	$-0.302^{+0.039}_{-0.030}$
	WFC/F814	$1.881^{+0.275}_{-0.223}$			$50.79^{+0.24}_{-0.24}$	$4.09^{+0.08}_{-0.09}$	$3.68^{+0.12}_{-0.11}$	$3.46^{+0.15}_{-0.14}$	$0.838^{+0.030}_{-0.035}$	$1.438^{+0.030}_{-0.040}$	$9.38^{+0.14}_{-0.13}$	$-0.061^{+0.126}_{-0.044}$
GC6	WFC/F606	$1.918^{+0.244}_{-0.237}$	K66	$5.51^{+0.06}_{-0.06}$	$50.75^{+0.21}_{-0.23}$	$4.24^{+0.06}_{-0.06}$	$3.93^{+0.07}_{-0.07}$	$3.71^{+0.07}_{-0.07}$	$0.868^{+0.026}_{-0.029}$	$1.458^{+0.027}_{-0.029}$	$9.02^{+0.07}_{-0.08}$	$0.096^{+0.039}_{-0.042}$
	WFC/F814	$1.918^{+0.244}_{-0.237}$			$50.76^{+0.21}_{-0.23}$	$4.24^{+0.06}_{-0.06}$	$3.93^{+0.07}_{-0.07}$	$3.70^{+0.11}_{-0.11}$	$0.868^{+0.026}_{-0.029}$	$1.458^{+0.026}_{-0.031}$	$9.03^{+0.11}_{-0.11}$	$0.096^{+0.057}_{-0.036}$
GC7	WFC/F606	$2.441^{+1.121}_{-0.573}$	K66	$4.85^{+0.17}_{-0.12}$	$49.35^{+0.66}_{-0.47}$	$3.46^{+0.17}_{-0.12}$	$3.11^{+0.17}_{-0.13}$	$2.79^{+0.17}_{-0.12}$	$0.492^{+0.082}_{-0.059}$	$1.093^{+0.082}_{-0.060}$	$8.94^{+0.17}_{-0.13}$	$0.413^{+0.097}_{-0.065}$
	WFC/F814	$2.441^{+1.121}_{-0.573}$			$49.16^{+0.66}_{-0.47}$	$3.46^{+0.17}_{-0.12}$	$3.16^{+0.18}_{-0.13}$	$2.98^{+0.17}_{-0.12}$	$0.467^{+0.083}_{-0.059}$	$1.062^{+0.082}_{-0.060}$	$8.80^{+0.17}_{-0.13}$	$0.540^{+0.135}_{-0.065}$
GC8	WFC/F606	$1.897^{+0.387}_{-0.215}$	K66	$5.42^{+0.08}_{-0.06}$	$50.58^{+0.32}_{-0.21}$	$4.36^{+0.08}_{-0.06}$	$4.21^{+0.09}_{-0.06}$	$3.75^{+0.09}_{-0.06}$	$0.849^{+0.041}_{-0.028}$	$1.449^{+0.041}_{-0.029}$	$8.90^{+0.10}_{-0.07}$	$0.436^{+0.046}_{-0.026}$
	WFC/F814	$1.897^{+0.387}_{-0.215}$			$50.20^{+0.32}_{-0.21}$	$4.36^{+0.08}_{-0.06}$	$4.35^{+0.09}_{-0.07}$	$3.82^{+0.09}_{-0.08}$	$0.775^{+0.041}_{-0.027}$	$1.384^{+0.041}_{-0.027}$	$8.84^{+0.10}_{-0.09}$	$0.808^{+0.046}_{-0.037}$
GC9	WFC/F606	$1.897^{+0.387}_{-0.215}$	K66	$5.05^{+0.08}_{-0.06}$	$49.64^{+0.32}_{-0.21}$	$3.03^{+0.08}_{-0.06}$	$2.23^{+0.09}_{-0.07}$	$2.65^{+0.08}_{-0.05}$	$0.504^{+0.040}_{-0.026}$	$1.066^{+0.040}_{-0.026}$	$9.28^{+0.09}_{-0.06}$	$-0.516^{+0.063}_{-0.049}$
	WFC/F814	$1.897^{+0.387}_{-0.215}$			$49.53^{+0.32}_{-0.21}$	$3.03^{+0.08}_{-0.06}$	$2.28^{+0.09}_{-0.06}$	$2.68^{+0.09}_{-0.06}$	$0.480^{+0.041}_{-0.026}$	$1.049^{+0.041}_{-0.027}$	$9.26^{+0.10}_{-0.07}$	$-0.398^{+0.046}_{-0.039}$
GC10	WFC/F606	$1.918^{+0.244}_{-0.237}$	K66	$5.49^{+0.06}_{-0.06}$	$50.49^{+0.21}_{-0.25}$	$4.61^{+0.07}_{-0.07}$	$4.69^{+0.09}_{-0.08}$	$3.70^{+0.16}_{-0.14}$	$0.848^{+0.026}_{-0.032}$	$1.470^{+0.028}_{-0.035}$	$9.00^{+0.15}_{-0.14}$	$0.938^{+0.067}_{-0.032}$
	WFC/F814	$1.918^{+0.244}_{-0.237}$			$50.36^{+0.21}_{-0.24}$	$4.61^{+0.07}_{-0.07}$	$4.74^{+0.09}_{-0.09}$	$3.74^{+0.22}_{-0.18}$	$0.823^{+0.026}_{-0.031}$	$1.447^{+0.027}_{-0.033}$	$8.98^{+0.20}_{-0.16}$	$1.063^{+0.080}_{-0.042}$